Characterization of the sub-surface architecture and identification of potential groundwater paths in a clay-rich floodplain using multi-electrode resistivity imaging.

Ander Guinea[1*], Suzanne Hollins[2], Karina Meredith[2], Stuart Hankin[2], Dioni I. Cendón[2,3]

[*]Corresponding author. Email address: a.guinea@federation.edu.au

[1] Federation University Australia, FoST, PO Box 663, Ballarat, VIC 3353, Australia.

[2] Australian Nuclear Science and Technology Organisation, Locked Bag 2001, Kirrawee, NSW 2232, Australia.

[3] Connected Waters Initiative, School of Biological, Earth and Environmental Sciences, The University of New South Wales, Sydney, NSW 2052, Australia.

Abstract

The interaction between surface water and groundwater in clay-rich fluvial environments can be complex and is generally poorly understood. Airborne electromagnetic surveys are often used for characterizing regional groundwater systems, but they are constrained by the resolution of the method. A resistivity imaging survey has been carried out in the Macquarie Marshes (New South Wales, Australia) in combination with water chemical sampling. The results have enabled the identification of buried palaeochannels and the location of potential recharge points. The data has been compared with previously published airborne electromagnetic data in the same area. Deeper less conductive features suggest that there is a potential connection between the Great Artesian Basin and groundwater contained within the shallow sand aquifer. Even though the chemistry of the groundwater samples do not indicate interaction with the Great Artesian Basin, the observed discontinuity in the saprolite implies potential for this to happen in other locations.

Key words: Electrical Resistivity Tomography, Recharge, Macquarie Marshes, Surface-groundwater interactions, Great Artesian Basin

1. *Introduction*

Climate change and anthropogenic influences have reduced the flow of the Macquarie River. The volume of water flowing through the Macquarie River at Dubbo (New South Wales, Australia) was reduced by half from 1980 to 2000 (Kingsford and Thomas 1995). Two major dams (Lake Burrendong and Lake Windamere) in the upper reaches of the Macquarie River have changed the natural flow regime of the river, decreasing the frequency and magnitude of the flow events into the Macquarie Marshes (Figure 1), with unknown long-term consequences to the Ramsar listed wetland. With the Macquarie Marshes facing environmental pressure, the conservation of the wetlands and an understanding of the interaction between surface water and shallow groundwater systems is essential.

The study of the groundwater recharge in the marshes is further challenged by the complex lithological heterogeneity associated with anastomosing fluvial systems (Miall 2014). In this setting, lithological interpolation between boreholes may lead to incorrect geological interpretations. Therefore, the description of the connectivity between surface water and groundwater must be supported by methods with a higher spatial coverage.

Formerly mainly used in mineral exploration, airborne electromagnetic (AEM) surveys are now regularly applied to regional hydrological studies worldwide (e.g. Viezzoli *et al.* 2010, Faneca Sanchez *et al.* 2012, Oldenborger *et al.* 2016). This technique measures the electrical conductivity response of the aquifer sediments, which is largely affected by its water content and salinity. AEM surveys are considered to provide information on the pathways for groundwater flow, which allows for better understanding of hydrological processes (Kirkegaard *et al.* 2011).

Alternatively, ground-based electrical resistivity methods can also provide the insight needed to characterise shallow alluvial materials (Chambers et al. 2014, Loke *et al.* 2013, Slater 2007, Revil *et al.* 2012). Direct current (DC) multi-electrode geoelectrical methods like electrical resistivity tomography (ERT) have been widely applied in the past to groundwater studies (e.g. Sharma and Baranwal 2005, Befus *et al.* 2011, Meyerhoff *et al.* 2014, Uhlemann et al. 2016). Even though AEM has much greater coverage capacity than any ground-based technique such as ERT, the latter has a significantly better resolution, which can be crucial in defining surface-groundwater processes in areas of hydrological significance.

In any case, because geophysical techniques are indirect methods, the data obtained can be more reliably interpreted when combined with chemical characterisation of water and geological description of the studied area (Schürch and Buckley 2002). Besides providing complementary data, hydrochemistry can help to resolve ambiguities in the interpretation of resistivity sections (e.g. low resistivity can be caused by presence of abundant clay or by high salinity of groundwater).

The aim of this study is to analyse the advantages and limitations of ERT in identifying potential surface water and groundwater interactions in clay-rich fluvial systems in comparison to AEM surveys.

2. *Study Area*

2.1 Geomorphology of the Macquarie Marshes

The Macquarie Marshes cover approximately 200 km^2 of the Macquarie River flood plains. These marshes are listed as wetlands of international importance under the Ramsar Convention for containing rich ecosystems and parts of them became nature reserve in 1971 (Robertson and Watts, 1999, Saintilan and Overton 2010). The marshes are one of the largest remaining inland semi-permanent wetlands in south-eastern Australia (Hollins *et al.* 2009). In spite of this, the diversity of fauna and flora has decreased in the wetlands while the flood-drought cycles (Figure 2) controlling these ecosystems have been severely affected by recent human activity (Hogendyk 2007).

Ralph and Hesse (2010) described the main geomorphological features of the Macquarie River and the Macquarie Marshes; the lower reach of the modern Macquarie River splits into numerous anastomosing and distributary channels that feed the floodplain wetlands and floodouts. The amount of flow in the river is highly regulated and seasonal, being mainly sourced in winter by the release of stored water in the upper catchment and by flooding in either winter or summer months. Large flood events occur in the lower catchment on years with high precipitation. The most recent floods preceding the survey took place in 1974, 1990 and 2010 reaching a peak flow of 87 $m^3 s^{-1}$ at Carinda in 1990 (NSW 2015). The occurrence and extent of floods during the Quaternary have shaped the morphology and hydrological characteristics of the northern lowlands; higher and lower flows compared to the current ones are known to have taken place in the Late Pleistocene-Holocene. The characteristic sequence of sediment filling in these rives is the result of a transition from higher energy regimes and it is responsible for the modern distribution of the marshes (Ralph and Hesse 2010).

The North Marsh Nature Reserve is a complex set of channels and dense vegetation (Figure 1) in which during floods the water flow slows considerably while seeping overbank (Ralph and Hesse 2010). Most of the water entering the marshes does not reach the channels downstream because of evapotranspiration, storage and groundwater recharge on the wetland. Few studies have described the interaction between the floodwater and the groundwater in the area and at present, limited information on groundwater recharge and surface water exchange is available (Hollins *et al*. 2009). Groundwater recharge is considered to take place mainly on the alluvial valley upstream, while recharge through infiltration of floodwater in the Macquarie Marshes area is thought to be more limited (CSIRO 2008).

2.2 Geological Setting

The marshes are situated on almost flat land, with a heterogeneous substrate consisting primarily of Cenozoic aged alluvium sand bodies overlain by thick floodplain and channel clay and silt deposits. The sand bodies appear irregularly distributed and in some areas, they are embedded in the predominant mud. Soils are generally made of heavy grey clay (Hollins *et al.* 2009). The Cenozoic deposits in the marshes overlie a cretaceous saprolite of variable thickness (20-40 m) formed within Rolling Downs Group (Kellet *et al.* 2006). This saprolite consists mainly of different types of clay (kaolinite on top with a transition to illite and smectite).

The saprolite is overlying unweathered Cretaceous Rolling Downs Group. This group outcrops approximately 30 km west of the studied area (Martin 1999) and is mainly composed of semiconsolidated grey and brown clays and siltstone, but fine clayey quartz sandstone and conglomerates are also present (Meakin *et al.* 1996). In the studied area, the Rolling Downs Group attains a thickness of approximately 120 metres (Macauley and Kellet 2009). The Cretaceous sequence overlies the Dridool and Keelindi Beds s (both containing important amount of sand mixed with finer sediments), which lie on top the Jurassic Pilliga Sandstone (Wolfgang 2000).

Initially, the only significant recharge of the shallow Cenozoic aquifer was considered to be leakage from the Macquarie River and floodplains (Pirard 1974), but later some authors suggested possible upwards recharge from the Great Artesian Basin (GAB) as demonstrated in other regional alluvial systems (Iverach et al. 2017). This basin is the largest groundwater reservoir in Australia and is represented in this area by the Pilliga Sandstone (Brereton 1994, Habermehl 1984, Wolgang 2000). However, Macauley and Kellet (2009) disregarded upwards recharge from the GAB in the Macquarie Marshes due to the widespread continuity of the saprolite layer (aquitard) observed in regional AEM data.

2.3 Study site

The area of study is located in the North Marsh Nature Reserve of the Macquarie Marshes (Figure 1). The area has a semi-arid climate with a mean rainfall of approximately 440 mm/year and potential evaporation of approximately 2,000 mm/year (Figure 3). Rainfall varies but in general, summer is the wettest season (Australian Bureau of Meteorology). The average monthly minimum temperature of 4.0 ˚C occurs in July and the average monthly maximum temperature of 34.7 ˚C occurs in January.

The studied transect comprises an east-west line of about 4 kilometres west from Bora channel (Figure 4). There is a noticeable change in the vegetation along this transect, being mainly dry grass in the western end and with a sharp transition about 1 kilometre east from Carinda Road to a more vegetated area (Figure 4A). After this visible boundary, the vegetation gets denser (Figure 4B) with increasing presence of surface water in ponds and creeks (Figure 4C). This transect represents the transition between the waterlogged area to the dry boundaries of the marshes (west end) at the time of the study. However, the position of the channels and the distribution of the vegetation can change drastically between flood events (Hogendyk 2007).

The resistivity imaging survey took place after the flood event of February 2011, which is the 4th most important on record after the floods of 1990, 1998 and 1950 respectively (Figure 3). Before the flood event, Australia had undergone the so-called *Millennium Drought*, which took place during the first decade of the 21st century. This drought is considered the worst on record for south-eastern Australia (van Dijkt *et al.* 2009). Even though the rainfall records in Carinda for that period do not show a particularly low rainfall in comparison with previous years, the catchment of the Macquarie River was receiving little rain and most of the potential runoff was retained at Lake Burredong (Figure 1). This is evidenced by the discharge records of the Macquarie River in the same location (Figure 3).

3. Methods

3.1 Electrical imaging

DC resistivity methods were employed in order to determine the electrical conductivity/resistivity distribution of the subsurface at the study site. An electrical current is injected on the surface of the terrain by two electrodes and the voltage difference between two other electrodes is measured. Increasing the spacing between electrodes also increases the depth of investigation. In 2D multi-electrode surveys, this measurement is performed repeatedly along a profile, obtaining apparent resistivity data points at different depths. In order to convert the apparent resistivity (or pseudosection) obtained in the survey into calculated real resistivity, an inversion routine is generally applied to the data (Loke *et al.* 2013). From this process, a trapezoid-shaped resistivity section is obtained. The electrical resistivity distribution showed by this image can be interpreted as soil layers and aquifers using the previous knowledge of the hydrogeology of the area. More detailed reviews on principles of geoelectrical methods and its practical applications can be found in Slater (2007), Revil *et al.* (2012) and Loke *et al.* (2013) among others.

The geophysical survey was performed during winter (7th to 10th of June) 2011. Three electrical resistivity tomography (ERT) profiles were acquired in this survey (Figure 4). The resistivimeter used for the data acquisition was an ABEM Terrameter SAS 1000/4000 with external power supply. Four cables with ~~16~~ 18 electrodes each (~~64~~ 72 in total) were connected to the main unit in sets of two. The spacing between electrodes was 5 metres, extending the length of the normal array to 360 metres. Different electrode arrays are commonly used in electrical prospection (Dahlin and Zhou 2004); in this study, all sections were obtained using the Wenner-Schlumberger array. This array is commonly used in hydrological studies due to its good depth of investigation, vertical resolution and low noise rate (Guinea *et al.* 2013). This array was implemented with a dipole length (a) of 5 m, 10 m, 15 m, and 20 m and a dipole separation factor (n) of ~~5~~ 1 to 8 for a total of 26 data levels. In order to extend the main section (ERT1; Figure 4) along the studied transect, the roll-along technique was used. This method increases the length of the section but does not increase the depth of investigation (Loke *et al.* 2013). ERT1 was obtained in three different stages and the data was combined afterwards, containing 5827 apparent resistivity data points. ERT2 and ERT3 (Figure 4) are located parallel to ERT1, but 50 metres north and south from its position respectively. Their exact location was decided after processing and interpreting the data of ERT1 and will be further discussed later. ERT2 and ERT3 were measured using Wenner-Schlumberger array without roll-along. The data was inverted using the commercial software RES2DINV (Geotomo Software, Loke and Barker 1996), which uses the smoothness-constrained least-squares method (deGroot-Hedlin and Constable 1990, Sasaki 1992). The discretization of the data consisted of 20 model layers with the thickness of each layer increasing a factor of 1.5 with depth and block lateral size of 5 m (same as electrode spacing) for a total of 4193 model blocks in the inversion of ERT1. The Jacobian matrix was recalculated after each iteration. The inversion employed a L1-norm for the data misfit and model roughness (Loke and Barker, 1996).

As ERT1 was recorded in three stages, there are two deep areas of the profile not covered by the apparent data ~~and therefore the resistivity there has been interpolated during the inversion process~~. These areas can be observed in the apparent resistivity section (Figure 5) and they are of no relevance for this study. Stacking data errors >5% were removed before the inversion. After that, a first inversion of the data was run and the percentage difference in apparent resistivity was calculated. Most of the section showed a percentage difference of >3% for depths below 30 metres. For depths higher than 30 metres, the percentage difference was higher with localized very high percentage differences. Some data points in these problematic deep areas showing apparent resistivity significantly different from neighbouring data points were removed. After filtering the data, t~~T~~he root mean square (RMS) deviation of the profile inverted as a single data ~~and~~ set ~~after 7 iterations is~~was 4.9% after 7 iterations; just below the recommended 5% (Loke *et al.* 2013).

3.2 Forward modelling

In addition to the resistivity survey, a synthetic resistivity model was calculated using RES2DMOD software, which calculates the electrical apparent resistivity pseudosection for a user-defined 2D underground model (Loke 2002). This software simulates the acquisition of field data in a theoretical terrain of user-defined resistivity distribution (e.g. Cornacchiulo and Bagtzoglou 2004, Sumanovac and Dominkovic 2007, Guinea *et al.* 2014). The pseudosection of the synthetic model was calculated using identical parameters to those used in the field data acquisition (i.e. electrode spacing, array, etc.). 6% of ~~uniformly~~ Gauss distributed random noise was added to pseudosection to represent the RMS error of the field data. The apparent resistivity data resulting from the forward modelling was then inverted using RES2DINV software using the same parameters as the ones applied in the inversion of field data. After 7 iterations, the RMS error of the inverted model data was 4.8%; very similar the RMS error obtained in the field data inversion.

The aim of the modelling is ~~to support the interpretation of the field data by creating a model depicting the main features identified in the resistivity sections and in accordance with what it has been observed in the regional drilling~~to validate the interpretation of the field data sections with particular emphasis to the connection between different levels and resistive features. If the interpretation is correct, the model should generate a distribution of apparent resistivity relatively similar to that of the field data and the product of the inversion should display similar features to those identified in the field resistivity section. However, it has to be considered that the model is a simplified version of the field data and therefore certain deviation between both data sets can be expected.

Alternative scenarios with slightly different connection patterns were modelled too (not shown), but these were discarded because they did not resemble the results of the field data as much as the model presented. As a result, these alternative interpretations can be ruled out.

3.3 Water and soil analysis

Samples of soil 1:5 soil water extracts from the unsaturated zone, surface water from the Bora Channel, Ginghet Creek and groundwater from site piezometers MQM29, MQM32 and MQM54 (Figure 3) were collected in December 2007, February 2008, April 2008, October 2008, March 2009 and June 2011. Soil samples from December 2007 and February 2008 were collected from three intervals throughout the soil profile (0 m, 0.5 m and 1.0 m below ground surface). Two deeper soil profiles were collected during April 2008 from MQM32 borehole. A further two deep profiles were collected during October 2008 and June 2011 from MQM32 and GCK (adjacent to the Ginghet Creek anabranch), down to the water table.

Duplicate soil samples were collected, using a hand auger, from 0.5 m intervals down the soil profile for characterisation, 1:5 soil water extracts and moisture % analysis. All soil samples were placed into sealed glass jars, and refrigerated until analysis. Soil water extracts were used to identify the water-soluble constituents in the soil sample and thus identify the salinity distribution in the soil profile. Soil water extracts were performed at 1:5 dilutions on soil samples. This methodology was developed by the USA Salinity Laboratory staff and is summarised in Rayment and Higginson (1992). Duplicate samples were prepared with one sample used for EC1:5 determination and a second sample filtered through a 0.45 µm Millipore TM cellulose acetate membrane filter and analysed for Cl using Ion Chromatography (IC). Fluid EC results are given in ohm·m instead of µS/cm in order to make them directly comparable with the resistivity imaging.

Surface water samples from the Bora Channel, Ginghet Creek and groundwater samples from site piezometers MQM29, MQM32 and MQM54 (Figure 4) were collected in December 2007, February 2008, April 2008, October 2008, March 2009 and June 2011. Standing water levels in the piezometers were measured followed by the purging of three well volumes and/or stabilisation of field parameters including Electrical Conductivity (EC), Oxidation-Reduction Potential (ORP), Dissolved Oxygen (DO), temperature and pH. Groundwater samples were collected from a bailer and filtered through a 0.45 µm, high volume filter. Surface waters were collected (when present) from the Bora Channel and Ginghet Creek (anabranch) at points nearest to sampling sites. Samples for Cl were collected in 125 ml HDPE (High Density Poly-Ethylene) and analysed by Ion Chromatography (IC).

4. Results

4.1 Electrical imaging

The results from ERT1 (Figure 5) show vertical and lateral variations of bulk resistivity, three main units can be identified (Figure 5A):

-*Top Unit*: The top unit is a low-resistivity (1 to 6 ohm-_m) continuous layer about 5 meter thick on average, but this thickness is variable and becomes thinner eastwards. The resistivity of this unit is relatively homogenous though it does increase locally at some points (Figure 5B). The Surface water samples collected in the Ginghet Creek area at the time of the resistivity survey display a conductivity value between 500 and 550 µS/cm (18-20 ohm-_m) and ponded water samples taken close to MQM32 display conductivity values close to 750 µS/cm (13 ohm-_m). Those values correspond to fresh water.

-*Middle Unit*: Below the Top Unit electrical resistivity increases (6 to 20 ohm-_m) down to a depth of approximately 20 metres (the depth is variable along the profile). This unit is discontinuous laterally, forming lenticular structures (Figure 5A, the structures in the image resemble circles rather than lenses due to the vertical exaggeration) and in general becoming increasingly connected and resistive from west to east. In fact, at the eastern end the lens-like structures coalesce and the high resistivity is more continuous (Figure 5D).

-*Bottom Unit*: Below a depth of 20 to 25 metres, the resistivity decreases to values similar to those of the Top Unit. The regional AEM data (Macauley and Kellet 2009) suggests that this deeper unit is thicker and continues below the maximum investigation depth (60 m). Even though the resistivity of this unit is predominantly low, there are some highly resistive anomalies within it (Figure 5C).

Sections ERT2 and ERT3 were measured parallel to ERT1, 50 meters north and south respectively (the location of ERT2 and ERT3 is indicated on Figure 4). These provide a tridimensional understanding of: *1*- The disconnected lens-like structures of the Middle Unit (Figure 5A) and its transition to more continuous high resistivity lenses; *2*- The nature of the high resistivity anomalies of the Bottom Unit (Figure 5C); and *3*- The connectivity between high resistivity anomalies in the Top Unit and the Middle Unit (Figure 5B).

Figure 6 shows the inverted sections of ERT2 (Figure 6A) and ERT3 (Figure 6C) and the correspondent segment of ERT1 located between them (Figure 6B). The main features have been labelled with numbers. *0*, *1*, *2* and *3* represent differentiated lenses previously identified in ERT1. *4* is a shallow high-resistivity feature connected in depth with the eastern Middle Unit indicated by *5* (Figure 5B) and *6* is a high-resistivity body within the Bottom Unit.

Both ERT2 and ERT3 have similar characteristics to those observed in the correspondent section of ERT1. The main differential feature of ERT2 (Figure 6A) is the lateral connectivity between the resistive bodies *1*, *2* and *3*, which in ERT1 appear separated (Figure 6B). Additionally, there seems to be a connection between *3* and *6* that is not observed in ERT1. The Middle Unit on ERT3 (Figure 6C) is more similar to that of ERT1; however, the position of *0*, *1*, *2* and *3* is shifted laterally. Even though the lens-like structures are separated, there seems to be a connection between *0* and *1*. Remarkably, *6* is absent in ERT3, suggesting this feature is dipping south.

4.2 Forward modelling

A synthetic model was designed using the resistivity section in Figure 6B as reference because most of the features described in the previous section are contained in it (Figure 7A). The resistivity value selected to represent the top and bottom units is 3 ohm- m because in ERT1 it ranges between 1 and 6 ohm m. A high resistivity feature (100 ohm m) was represented in the top unit similar to feature *4* in Figure 6B. The resistivity values selected for the lenticular features in the middle unit were 10 and 15 ohm m, based in the values that they display in the inverted section of ERT1. The lenses are disconnected in the western side of the model and they are connected by a 10 ohm m background in the eastern side of the model. Finally, feature *6* in Figure 6B was represented as an irregular deep level with high resistivity.

The pseudosection calculated by forward modelling (Figure 7B) has ~~some~~ significant similarities to the analogous section of the pseudosection in Figure 5. In particular a vertical high apparent resistivity distribution underneath feature *4* and the general higher apparent resistivity in the middle unit to the east. As mentioned before, the two pseudosections have divergences due to one of them being based on a model and due to the challenge of representing adequately feature *6* in the model. The latter point is discussed further in section 5.3. The inversion results of the synthetic data set (Figure 7C) are very similar to the equivalent section of ERT1, which validates the interpretation of the main key features.

4.3 Water and soil analysis

The surface water samples collected after the 2011 flood event (Figure 8, data points with different shades of blue) show a very similar composition, including the sample taken upstream the Macquarie River (Gibson's way) which indicates that the chemical composition of surface water doesn't change significantly when crossing the marshes. Older surface water samples show relatively similar composition, though one sample from Bora Creek and another sample from Ginghet Creek collected on early 2008 are enriched in bicarbonate (Figure 8).

The groundwater samples collected in piezometers MQM32 and MQM54 (Figure 4) during the resistivity survey are enriched in Na^+ compared to the surface water samples. On the other hand, the anionic composition of groundwater in MQM32 is closer to surface water samples than that in MQM54, which is notably enriched in Cl^- and SO_4^{2-}. The temperature of the groundwater in MQM32 is also closer to surface water than in MQM54 (14.87 ˚C and 16.20 ˚C respectively), with the surface water being approximately 7 ˚C on average at the time of the survey). The total head at the time of the study was Australian Height Datum (AHD) 135.1 m in MQM54 (bore elevation AHD 140) and AHD 141.2 m in MQM32 (bore elevation AHD144).

The deep soil profiles from Ginghet Creek (GCK) and MQM54 (Table 1) show a composition dominated by heavy clay down to 4.5 metres. Below, the soil is still dominated by clay but with some sand partings. In the GCK log, clean sand is found at a depth of 9 metres and the soil is saturated in water at 7.5 metres and below. Unlike the log from GCK, clean sand is not found at 9 metres below the surface in the MQM54 log, but the content of sand increases with depth and the soil is saturated below 8.5 metres. The soil log from MQM32 (nearby GCK) only goes down to 6 metres and is mostly made of heavy clay.

The Cl^- content of the analysed samples of the soil logs show a variable distribution (Figure 8). The Cl^- content of GCK for the first meter of soil is low, but it rapidly increases to more than 350 mg/L between 1.5 and 3.5 meters deep, falling down to contents below 100 mg/L at a depth of 4 metres and decreasing steadily down to about 20 mg/L. The samples from the nearby MQM32 log have a similar content in Cl^- to those of GCK for the first meter of the soil and below a depth of 4 metres, but they don't show the previously described high content for depths between 1.5 and 3.5 metres. The log of MQM54 displays a similar trend to that of MQM32, but with much higher content in Cl^- in deep samples (4 metres deep and below). The results obtained from the fluid $EC_{1:5}$ extracts show a variable but relatively low conductivity within the first 2.5 metres of MQM32 and GCK (Figure 9) and a sharp rise in both logs at 3 m in depth.

Below three metres $EC_{1:5}$ decreases progressively with depth, most notably below 8 metres. The bulk resistivity of the soil (obtained from the electrical resistivity tomography profile at the location of EM32) also displays a rise in conductivity at 3 metres (drop in resistivity) deep and a drop below 8 metres deep, with a similar general trend to that of the $EC_{1:5}$ for EM32 and GCK. The $EC_{1:5}$ of MQM54 is in all cases higher than that of the other two logs for samples at similar depth, which is coherent with the higher content in Cl^-. The results from the $EC_{1:5}$ and the Cl^- are indicative of the salinity present in the soil samples and consistent with the bulk resistivity in the top unit.

4.4 Limitations of electrical imaging in a clay dominated environment

Resistivity methods have been widely used to describe the architecture of more energetic floodplains (e.g. Crook *et al.* 2008, Burton *et al.* 2014, Grygar *et al.* 2016), but in low energy environments this is challenging due to the overlap in resistivity between the dominating clay and sandy layers containing saline groundwater. In this section, the results from the resistivity survey and the soil and groundwater samples collected during the geophysical campaign are analysed and compared with other data sets from catchments of similar characteristics.

The comparison of the $EC_{1:5}$ and Cl^- content from the log-samples with the bulk resistivity obtained from the electrical imaging at GCK (Figure 9) shows a correlation between the salinity and the bulk resistivity. Within clay-dominated layers, minor compositional changes down to a depth of 8 meters (Table 1) have little impact in bulk resistivity and its variation is dominated by the salinity. In any case, the resistivity remains below 7 ohm-_m in all clay-dominated layers independently of the salinity. Therefore, bulk resistivity values of 7 ohm-_m or less can be interpreted as clay-dominated materials with different salinity contents (lower resistivity indicating higher salinity). Below a depth of 8 metres the sand composition increases notably and at that same depth the bulk resistivity increases accordingly to more than 7 ohm-_m (Figure 9). However, the $EC_{1:5}$ decreases for deeper sandy clay samples (Table 1), indicating a reduction in salinity and showing that salinity is also a relevant factor in the bulk resistivity of those levels.

The bulk resistivity of similar clay-dominated fluvial deposits in Australia has been measured by using electromagnetic induction logs (EM39) in boreholes (Kellet *et al.* 2008, Andersen and Acworth 2009, Guinea *et al.* 2013). In these studies, sand-rich units with brackish to fresh water display bulk resistivity values above 7 ohm-_m. Resistivity values under that threshold correspond mostly to clay-dominated layers. However, the records by Kellet et al. (2008) show that in the presence of saline water, (indicated by measurements of EC of recovered mud) sandstone layers cannot be identified only by their bulk resistivity. In the case of clay dominated layers, the bulk resistivity values in the logs is always below the threshold of 7 ohm-_m. Andersen and Acworth (2009) attribute any value of bulk conductivity over 1600 µS/cm (<6.3 ohm m) in the Maules Creek catchment where the study takes place, to be caused by clay layers.

These values match up perfectly with the results of the resistivity imaging described in section 4.1. Comparing all the data available we can conclude that in the studied area, bulk resistivity values above 7 ohm m correspond to sand-dominated deposits with brackish to fresh groundwater. In Kellet et al. (2008), sand rich layers with drilling-mud conductivities above 1500 µS/cm are indistinguishable from clay layers. However, the mud was recovered in an open system and therefore the conductivity recorded is inaccurate.

In this study, groundwater samples from MQM32 had an EC of 4370 µS/cm and TDS of 3580 mg/L in layers where the ERT profile displays resistivity values between 8 and 9 ohm m. On the other hand, groundwater samples from MQM54 had an EC of 13 904 µS/cm and TDS of 11 499 mg/L at the time of the geophysical survey. In the area where MQM54 is located, the resistivity in the ERT profile is between 5 and 6 ohm m.

Papp *et al.* (2014) also used ERT in a clay-dominated area of the Lower Murrumbidgee catchment (NSW, Australia). Clay-rich and sand-rich layers containing brackish groundwater (5643 µS/cm) display bulk resistivity values below 7 ohm m. On the other hand, two samples from clayey sand layers containing lower salinity groundwater of 1278 and 3405 µS/cm, display bulk resistivity ranges of 12.5-14.5 and 9.3-10.7 ohm m, respectively. Figure 10 displays the data obtained by Papp et al. (2014) together with the data obtained in this study. The bulk conductivity for clay-rich layers do not present a clear trend with varying fluid EC, but in the case of sand rich layers there is a general increase in bulk conductivity as the fluid EC decreases.

In summary, results from resistivity imaging surveys and soil-water chemistry in clay dominated low-energy fluvial environments, show that layers with resistivity values above 7 ohm m are indicative of sand containing brackish to fresh groundwater. Lower resistivity values will indicate clay; however, sandy bodies with highly saline water content are missed.

5. Discussion

5.1 Surface water/shallow groundwater interactions

In section 4.1, three units have been defined from the results of ERT1 (Figure 5A). The low-resistivity Top Unit corresponds with sediments such as clay that have accumulated from low energy overbank flow in the area. The resistivity increases locally due to sand deposited by active surface channels that can be identified as resistive (>20 ohm-m) features (Figure 5B), but in general this unit is made of clay-dominated layers. The thinning of this layer towards the east could be related to erosive processes in the active part of the marsh. The Middle Unit represents a complex shallow aquifer system with irregularly distributed sand. The presence of sand is the main reason higher resistivity values are observed, however, as discussed before, the salinity of the water content has to be taken into consideration here.

The existence of the clay-rich Top Unit at the study site is suggested to inhibit groundwater recharge from surface water into the shallow aquifer, though recharge could still happen through tree roots and clay cracking features. The results from the resistivity imaging also suggest that the connection between surface water and groundwater is limited because of the clay. However, local increases in resistivity within the Top Unit indicate the presence of sand that could facilitate downwards recharge. This is the case of a thick surface channel in the Top Unit at distance: 750 to 850 m in ERT1 (Figure 5B). At this point, the lack of resistivity values below 7 ohm-m suggests that there is little clay between the western end of the channel and the Middle Unit. The reason why this sandy channel is particularly thick could be related to scouring during big flood events in deeper channels or due to channel convergence (Cendón *et al.* 2010). This would be a major recharge point for the groundwater in this area and continues both in northerly and southerly directions since the same feature is observed in ERT2 and ERT3. In Figure 6 it can be appreciated from the resistivity distribution that the recharge point (*4*) is feeding the groundwater only to the east (*5*) since the palaeochannel to the west (*3*) appears disconnected (Figure 11). This is further supported by the synthetic model (Figure 7); if feature *4* in the initial model is not directly connected to the surface channel, this is, a layer of clay (3 ohm-m) is represented between the surface channel and the sand level below (Figure 7A), the inversion of the data shows them disconnected (data from alternative models is not included).

In ERT3 (Figure 6C) there is a potential recharge point of groundwater from the surface between the palaeochannels *1* and *2*. This recharge point is not present in ERT1 (Figure 6B) but it is observed downstream in ERT2 (Figure 6A). Nevertheless, the yet relatively low resistivity (4-6 ohm m) at this point indicates the presence of a significant amount of clay and therefore the amount of surface water seeping to the groundwater would not be significant unless recharge is driven by non-lithological features.

As a whole, the eastern half of the Middle Unit in ERT1 (Figure 5) seems to be better connected with the surface water than the western half. This is coherent with the higher salt content found in groundwater from MQM52 compared to that from MQM32. The major ion chemistry of water samples (Figure 8) also supports this interpretation since MQM32 is closer to the composition of surface water samples than MQM54, suggesting surface water recharge in the area of Ginghet Creek. The major ion chemistry of the samples collected in MQM30 and MQM29 (Figure 4) during 2007 and 2008 (Figure 8) are closer to that of MQM54, suggesting limited recharge from the surface in the Bora Channel area, though this is slightly outside of the resistivity imaging survey area.

A potential recharge point after a flood event is observed in ERT at distance: 1400 to 1425 m (Figure 5D). This is because the surficial layer of clay seems to be thin enough that during a flood event the channel could be scoured allowing water to seep into the aquifer below.

5.2 Characteristics of the shallow groundwater system

At the eastern end of the Middle Unit, the higher resistivity materials are quite continuous and, though there are local decreases in resistivity probably related to the higher clay content, this unit appears to be sand-rich and therefore can be interpreted to be permeable. From the east to the centre of the Middle Unit, the resistivity decreases possibly due to a decrease in grain size, but the characteristics of the unit appear to be relatively continuous. Further west, resistivity contrast within the Middle Unit increases, defining individual palaeochannels (lens-like features) surrounded by lower resistivity materials (Figure 11). The channels are likely to represent the anabranches of a buried braided river (Ralph, 2008) and they are similar to the river system that is currently observed on the surface of the marshes. The low resistivity surrounding the palaeochannels (Figure 5A) represents clay levels deposited from overbank flow at the time when the palaeochannels were active and influence the connectivity of the shallow aquifer due to their low permeability. Consequently, the palaeochannels are apparently disconnected hydraulically from the more continuous eastern part of the Middle Unit.

The overall resistivity of the palaeochannels seems to decrease westwards, progressively blending with the clayey background. This might be related to a lower sand content to some extent, but the high electrical conductivity of a groundwater sample obtained at the time of the study on MQM54 (13 904 µS/cm), screened between 8.5 and 9.5 meters deep, compared to a sample from MQM32 for a similar depth (4370 µS/cm), indicates that the salinity of the groundwater is the main reason for the low electrical resistivity in this case. The lower resistivity in those channels is an indication of their degree of isolation and increased groundwater salinity.

The main features of the Middle Unit are also observed in ERT2 and ERT3 (Figure 6). The lens-like structures labelled as *0*, *1*, *2* and *3* represent differentiated palaeochannels observed in ERT1. In ERT2the palaeochannels *1*, *2* and *3* appear to be connected laterally and they are not well defined individually. In fact, the only isolated palaeochannel that can be identified in ERT2 is *0*, located at the western end of the profile. Moving upstream from ERT1 and ERT2, the section in ERT3 shows slightly different features. In this case, the palaeochannels *1*, *2* and *3* do not seem to be connected, similarly to what is observed in ERT1, but the palaeochannel *0* seems closer to *1*. In any case there probably is some degree of connection between the palaeochannels and the eastern Middle Unit due to the tridimensional variability of the distribution of the channels evidenced by ERT2 and ERT3 (Figure 6).

The non-linear nature of the palaeochannels observed on the resistivity sections is common on braided river systems. On the surface of the modern marshes, similar features can be observed; the channels move laterally along the direction of the river channel, connecting and disconnecting from other channels (Figure 2). The three dimensional non-linearity of the palaeochannels is likely creating some distortion in the inversion of two dimensional sections. In any case, their overall distribution and interconnectivity should not be affected significantly.

5.3 Local/regional resistivity and potential for GAB upwards discharge

The Bottom Unit in the ERT sections represents a very thick sequence of clays. Palamara *et al.* (2010) described this low-resistivity unit as the Cretaceous Saprolite of the Rolling Downs Group. For the most part, the resistivity imaging in this study does not show any evidence of sand content, suggesting this may be an aquitard unit. However, the ERT sections show localised high-resistivity features (Figure 5C). According to the local geology (Meakin *et al*. 1996), below the saprolite there is a transition to unweathered Rolling Downs Group. These deeper materials have higher resistivity due to the presence of sand and conglomerates. The Rolling Downs group is represented by feature *6* in the synthetic model as an irregular level of high resistivity (100 ohm m). The exact shape and resistivity values selected in the model are probably inaccurate due to most of the transition between the saprolite and the unweathered Rolling Downs Group being close to the maximum depth of investigation in this study, which limits the amount of information obtained in ERT1 regarding this unit. Due to the highly irregular nature of this transition, its depiction in the resistivity sections is possibly distorted by three-dimensional variations and likely to contain artifacts.

An AEM survey was carried out by Palamara *et al*. (2010) in the Macquarie Marshes and included a number of east-west flight lines. One of those lines passed over the area studied with the ERT (Figure 2). The comparison between both data sets show that in the AEM line the top and middle units are not well defined (Figure 12). The palaeochannels observed in the ERT are absent and the potential points for surface water infiltration cannot be identified. The saprolite layer is displayed at the same depth with both methods but, importantly, in the AEM data the saprolite appears continuous while with the ERT discontinuities have been identified (Figures 5C and 6A).

The transition between the saprolite and the unweathered Rolling Downs Group occurs at variable depths and is irregular in nature. This is also observed in this study in the ERT section, where the high resistivity anomalies of the Bottom Units are discontinuous laterally and appear at different depths (Figure 11).

Even though some authors suggested possible recharge of the shallow groundwater of the Macquarie Marshes from the GAB groundwater (Brereton 1994, Habermehl 1984, Wolfgang 2000), Macauley and Kellet (2009) considered that this mechanism was not possible due to the widespread continuity of the saprolite observed in the AEM data. However, the discontinuities observed by the electrical resistivity tomography sections in this study suggest that at some points there may be a connection between the unweathered Rolling Downs Group and the Middle Unit. In Figure 6A Palaeochannel *3* seems to be connected to the deep high-resistivity anomaly *6*. This connection is not observed southwards in ERT1 (Figure 6B) and, most notably, *6* is absent in ERT3 (Figure 6C). This indicates that these potential windows for recharge are very discontinuous.

The chemistry of the groundwater samples analysed (Figure 8) does not represent the typical composition the GAB. Isotopic analysis of groundwater at this site suggests a meteoric origin during flood events rather than deep upwards recharge (Hollins *et al*. 2009). Therefore, recharge from the GAB can be ruled out for this end on the Marshes, but the connection between unweathered Rolling Downs Group and shallow palaeochannels means that the possibility has to be considered in other locations.

Even though ERT cannot match the land coverage and data acquisition speed of AEM, its better resolution allows for a more detailed characterization of local hydrological processes. AEM surveys are often coupled with log records for quality control but borehole records are unidimensional and therefore do not constrain horizontal changes. Despite AEM being an adequate method to identify major regional hydrogeological units, its limitations need to be considered; we suggest that ERT can be used in target locations of AEM lines to improve interpretation.

6. Conclusions

Electrical Resistivity Tomography has proven to be an adequate method for describing the geometrical information of the subsurface in clay-rich fluvial systems. In the case study at the western end of the North Marsh Nature Reserve of the Macquarie Marshes, water chemical analysis have been compared with the resistivity data.

The analysis of the data in combination with data obtained in other catchments with similar characteristics has shown that values of resistivity below 7 ohm m correspond to clay-rich levels and values above that threshold are sand dominated with fresh to brackish water. However, sandy layers containing groundwater with elevated salinity cannot be distinguished from clay in the resistivity sections.

The surveyed area is characterized by a top layer of heavy clay below which there is an old braided river system that lies above the saprolite of the Cretaceous Rolling Downs Group. The sand contained in that buried system is distributed irregularly, forming relatively isolated palaeochannels on the western boundary of the flood plain with increasing connectivity towards the east. The groundwater in the old braided system is recharged from surface water that infiltrate sandy units in the clay that were created by modern river channels on the surface of the marshes. This recharge happens mainly in the eastern section of the studied area and, because of this, the water is substantially more saline in the western end.

Recharge from deep aquifer to the shallow of the marshes has been previously discarded due to the interpretation from an AEM survey of a continuous saprolite level below the Macquarie Marshes. However, the resistivity data obtained in this study has shown that the saprolite layer is not as continuous as it was thought and that there are potential windows for groundwater to flow upwards. The chemistry of the groundwater samples collected do not suggest mixing with water from the GAB in this location, but the observed discontinuity of the saprolite makes it possible for this to happen in other areas. Even though ERT cannot replace AEM for describing regional subsurface architecture, its higher resolution gives a more detailed view and can be used in combination with the latter in areas of hydrological significance.

Acknowledgements

The authors would also like to thank various Australian Nuclear Science and Technology Organization personnel such as Robert Chisari, Henri Wong, Barbora Gallagher and Chris Dimovski with their assistance in the field and/or groundwater analytical work. A Spanish government travel grant (CGL2009-11096) to the corresponding author facilitated the electrical resistivity profiles.

Captions:

Figure 1: Map of the Macquarie-Bogan basin. The area covered by the Macquarie Marshes is indicated in green (modified from Ralph and Hesse 2010). The insert shows the main channels of the Macquarie Marshes (shaded in green) and orange shading indicates the nature reserve areas of the wetlands. A red star represents the area of study.

Figure 2: Detail of the Macquarie Marshes floodplains, the inundation areas are represented with different colours based on their average flooding recurrence (modified from Commonwealth Environmental Water Office 2015). The Airborne Electromagnetic flight line 20990 by Palamara *et al.* (2010) is indicated by a white line.

Figure 3: Recorded discharge of the Macquarie River at Carinda (Bells Bridge) and daily rainfall records for the Carinda Post Office weather station from 1939 onwards. The date of the most important flood events are indicated on the correspondent peaks and the *Millennium Drought* period is highlighted.

Figure 4: Location of the main water sampling sites and the resistivity imaging lines. Sampling points named MQM (Macquarie Marshes) represent piezometers with screens in the shallow aquifer, while GCK (Ginghet Creek) is a surface water sampling point. Surface water was also sampled at other locations.

Figure 5: Apparent resistivity and inverted resistivity sections of ERT1. A) Detail of buried lens-like features, the boundaries between the main 3 units (Top, Middle and Bottom) are indicated by dotted red lines. B) Detail of a highly resistive surface feature in the Top Unit. C) Detail of highly resistive feature in the Bottom Unit. D) Detail of the high-resistivity anomaly produced by the shallow aquifer in a position very close to the surface.

Figure 6: Electrical resistivity inverted sections of ERT2 (A) and ERT3 (C) and the corresponding section of ERT1 (B). The main features are indicated by *0*, *1*, *2*, *3*, *4*, *5*, and *6*. The location of ERT2 and ERT3 is showed in Figure 4.

Figure 7: Synthetic resistivity model based on the interpretation of the inverted field data in Figure 6B. A) Resistivity distribution in the model. B) Pseudosection calculated by forward modelling. C) Inverted model of the theoretical apparent resistivity.

Figure 8: Piper diagram showing the major ionic composition of water samples collected in the studied area. Circles represent groundwater samples and triangles surface water samples. The blue coloured samples correspond to the 2011 campaign and the warm colours correspond to older samples (2007 and 2008). GCK1 and GCK2 correspond to samples collected at Ginghet Creek and the black square indicates the composition of rainwater at Creswell. The shaded areas indicate the typical composition-range of groundwater samples from the J Aquifer of the GAB (Fulton 2012). The location of the sampling points is indicated in Figure 4.

Figure 9: Cl^- and $EC_{1:5}$ measured in the log-cores drilled at MQM32, MQM54 and GCK. The results are compared with the bulk resistivity obtained with the resistivity imaging for similar depths. A synthetic lithological description of the cores from GCK and MQM54 is included. The location of the logs is shown in Figure 4.

Figure 10: Bulk resistivity results from samples analysed in this study (black data points) and data obtained by Papp *et al.* (2014) in the Lower Murrumbidgee catchment (NSW, Australia) using similar methods of study (grey data points). The triangles indicate sand-rich layers and the circles clay-rich layers.

Figure 11: Hydrogeological interpretation of part of the resistivity section ERT1. The main features are highlighted.

Figure 12: Modified transect of the Airborne Electromagnetic flight line 20990 by Palamara *et al.* (2010). The levels identified as saprolite and unweathered Rolling Downs Group are indicated in white and the section overlapping the resistivity profile ERT1 is indicated with a dotted square. The flight-path of the line is shown in Figure 2.

Table 1: Lithological composition of soil logs recovered from GCK and MQM54. Soil description is given in depth intervals of 0.5 metres. The location of the logs is indicated in Figure 4.

References

Andersen, M.S., and Acworth, R.I., 2009. Stream-aquifer interactions in the Maules Creek catchment, Namoi Valley, New South Wales, Australia. *Hydrogeology Journal*, 17, 2005–2021.

Befus, K.M., Cardenas, M.B., Ong, J.B., and Zlotnik, V.A., 2011. Classification and delineation of groundwater-lake interactions in the Nebraska Sand Hills (USA) using electrical resistivity patterns. *Hydrogeology Journal*, 20, 1483–1495.

Brereton, G., 1994. *Macquarie Marshes management strategy. Stage 1 – biophysical investigations*. Summary Report, Natural Resources Management Strategy.

Burton, B.L., Powers, M.H., and Ball, L.B., 2014. Characterization of subsurface stratigraphy along the lower American River floodplain using electrical resistivity, Sacramento, California, 2011: U.S. Geological Survey Open-File Report 2014–1242, 62 p.

Cendón, D.I., Larsen, J.R., Jones, B.G., Nanson, G.C., Rickleman, D., Hankin, S.I., Pueyo, J.J., and Maroulis, J.C., 2010. Freshwater recharge into a shallow saline groundwater system, Cooper Creek floodplain, Queensland, Australia. *Journal of Hydrology*, 392, 150–163.

Commonwealth Environmental Water Office, 2015. *Integrated planning for the use, carryover and trade of Commonwealth environmental water: Macquarie River Valley 2015–16*. Common Wealth of Australia.

Chambers, J.E., Wilkinson, P.B., Uhlemann, S., Sorensen, J.P.R., Roberts, C., Newell, A.J., Ward, W.O.C., Binley, A., Williams, P.J., Gooddy, D.C., Old, G., Bai, L., 2014. Derivation of lowland riparian wetland deposit architecture using geophysical image analysis and interface detection. *Water Resources Research*, 50, 5886–5905.

Cornacchiulo, D., and Bagtzoglou, A.C., 2004. Geostatistical reconstruction of gaps in nearsurface electrical resistivity data. *Vadose Zone Journal*, 3, 1215–1229.

Formatted: Font: Italic

Formatted: Font: Italic

Crook, N., Binley, A., Knight, R., Robinson, D.A., Zarnetske, J., and Haggerty, R., 2008. Electrical resistivity imaging of the architecture of substream sediments. *Water Resources Reesearch*, 44, W00D13.

CSIRO, 2008. *Water availability in the Macquarie–Castlereagh*. A report to the Australian Government from the CSIRO Murray–Darling Basin Sustainable Yields Project, CSIRO, Australia.

Dahlin, T., and Zhou, B., 2004. A numerical comparison of 2D resistivity imaging with ten electrode arrays. *Geophysical Prospecting*, 52, 379–398.

deGroot-Hedlin, C., and Constable, S., 1990. Occam's inversion to generate smooth, two-dimensional models from magnetotelluric data. *Geophysics*, 55, 1613–1624.

Faneca Sanchez, M., Gunnink, J.L., van Baaren, E.S., Oude Essink, G.H.P., Siemon. B., Auken, E., Elderhorst, W., and de Louw, P.G.B., 2012. Modelling climate change effects on a Dutch coastal groundwater system using airborne electromagnetic measurements. *Hydrology and Earth System Sciences*, 16, 4499–4516.

Fulton, S., 2012. *Technical Report: Great Artesian Basin Resource Assessment*. Department of Land Resource Management, Northern Territory Government, Report 14/2102A.

Grygar, T.M., Elznicova, J., Tumova, S., Famera, M., Balogh, M., and Kiss, T., 2016. Floodplain architecture of an actively meandering river (the Ploučnice River, the Czech Republic) as revealed by the distribution of pollution and electrical resistivity tomography. *Geomorphology*, 254, 41–56.

Guinea, A., Timms, W., and Acworth, R.I., 2013. Comparison between the hydraulic properties of two low-permeability alluvial systems supported by geophysical methods. Near Surface Geoscience 2013 - 19th EAGE European Meeting of Environmental and Engineering Geophysics, extended abstract. DOI: 10.3997/2214–4609.20131371.

Guinea, A., Playà, E., Rivero, L., and Salvany, J.M., 2014. Geoelectrical prospecting of glauberite deposits in the Ebro basin (Spain), *Engineering Geology*, 174, 73–86.

Formatted: Font: Italic

Formatted: Font: Italic

Habermehl, M.A., 1984. *The influence of the Great Artesian Basin on the Macquarie Marshes, NSW.* AGSO Environmental Geoscience and Groundwater Program, Canberra.

Hogendyk, G., 2007. *The Macquarie Marshes: an Ecological History*. Institute of Public Affairs, occasional paper.

Hollins, S., Meredith, K., and Twining, J., 2009. *Study of groundwater-surface interactions in the Maquarie Marshes and sources of water for riparian vegetation transpiration*. ANSTO report, Australia.

Iverach, C. P., Cendón, D. I., Meredith, K. T., Wilcken, K. M., Hankin, S. I., Andersen, M. S., and Kelly, B. F. J. 2017 ~~(in press)~~. A multi-tracer approach to constraining artesian groundwater discharge into an alluvial aquifer. *Hydrol. Earth Syst. Sci.*, 21, 5953–5969. ~~Discuss., https://doi.org/10.5194/hess-2017-327~~

Kellet, J., Mullen, I., Mansfield, D., and Spring, J., 2006. *Drilling and Geophysical Logging for Design of Airborne Electromagnetic Survey in the Lower Macquarie Valley, New South Wales, Australia*. A report to the Australian Government from the Bureau of Rural Sciences, Common Wealth of Australia.

~~Iverach, C. P., Cendón, D. I., Meredith, K. T., Wilcken, K. M., Hankin, S. I., Andersen, M. S., and Kelly, B. F. J. 2017 (in press). A multi-tracer approach to constraining artesian groundwater discharge into an alluvial aquifer. Hydrol. Earth Syst. Sci. Discuss., https://doi.org/10.5194/hess-2017-327~~

Kellet, J., Mullen, I., Mansfield, D., Spring, J., and Frost, M., 2008. *Drilling, Coring and Geophysical Logging for Calibration of Airborne Electromagnetic Survey in the Lower Macquarie Valley, New South Wales, Australia*. A report to the Australian Government from the Bureau of Rural Sciences, Common Wealth of Australia.

Kingsford, R.T., and Thomas, R.F., 1995. The Macquarie Marshes in Arid Australia and Their Waterbirds: A 50-Year History of Decline. *Environmental Management*, 19 (6), 867–878.

Formatted: Font: Italic

Formatted: Font: Italic

Formatted: Font: Italic

Formatted: Font: Italic

Formatted: Font: Italic

Formatted: Font: Italic

Kirkegaard, C., Sonnenborg, O., Auken, E., and Jørgensen, F., 2011. Salinity Distribution in Heterogeneous Coastal Aquifers Mapped by Airborne Electromagnetics. *Vadose Zone Journal*, 10, 125–135.

Loke, M. H., and Barker, R.D., 1996. Rapid least-squares inversion of apparent resistivity pseudosections by a quasi-Newton method, *Geophysical Prospecting*, 44, 131–152.

Loke, M.H., 2002. *RES2DMOD ver 3.0. 2D Resistivity and IP Forward Modelling*.~~In:~~ Loke Penang, M.H. (Ed.).

Loke, M. H., Chambers, J.E., Rucker, D.F., Kuras, O., and Wilkinson, P.B., 2013. Recent developments in the direct-current geoelectrical imaging method. *Journal of Applied Geophysics*, 95, 135–156.

Macauley, S., and Kellet, J., 2009. *Mapping groundwater and salinity using airborne electromagnetics in the Lower Macquarie River Valley, New South Wales*. A report to the Australian Government from the Bureau of Rural Sciences, Australia.

Martin, H., 1999. The stratigraphic palynology of the Macquarie River Valley, central western New South Wales. In: *Proceedings of the Linnean Society of New South Wales*. Vol. 121. pp. 113–127.

Meakin, S., Henley, H., Pocover, S., and Watkins, J., 1996. *Walgett 1:250 000 Geological Sheet, SH/55–11~~–, First~~ first edition*. Geological Survey of New South Wales, Sydney.

Meyerhoff, B.S., Maxwell, R.M., Revil, A., Martin, J.B., Karaoulis, M., and Graham, W.D., 2014. Characterization of groundwater and surface water mixing in a semiconfined karst aquifer using time-lapse electrical resistivity tomography. *Water Resources Research*, 50 (3), 2566–2585.

Miall, A., 2014. *Fluvial Depositional Systems*. Springer Geology~~, pp. 316~~.

NSW Department of Primary Industries (Office of Water) accessed on Dec 2015: http://realtimedata.water.nsw.gov.au/water.stm?ppbm=SURFACE_WATER&rs&3&rskm_org

Oldenborger, G.A., Logan, C.E., Hinton, M.J., Pugin, A.J.M., Sapia, V., Sharpe, D.R., and Russell, H.A.J., 2016. Bedrock mapping of buried valley networks using seismic reflection and airborne electromagnetic data. *Journal of Applied Geophysics*, 128, 191–201.

Palamara, D.R., Rodriguez, V.B., Kellet, J., and Macaulay, S., 2010. Salt mapping in the Lower Macquarie area, Australia, using airborne electromagnetic data. *Environmental Earth Sciences*, 61, 613–623.

Papp, E., Burraston, L., and McPhail, D.C., 2014. Identifying palaeochannels and their influence on groundwater systems in the Lower Murrumbidgee catchment, NSW. *HUNGEO extended abstracts*, 156-167, ISBN 978-963-8221-53-7.

Formatted: Font: Italic

Pirard, F., 1974. *Macquarie River Groundwater Investigations. Dubbo – Narromine – Trangie Section*. Bureau De Recherches Geologiques Et Minieres, Report.

Formatted: Font: Italic

Ralph, T.J., 2008. *Channel breakdown and floodplain wetland morphodynamics in the Macquarie Marshes, south-eastern Australia*. PhD thesis, Macquarie University.

Formatted: Font: Italic

Ralph, T.J., and Hesse, P.P., 2010. Downstream hydrogeomorphic changes along the Macquarie River, southeastern Australia, leading to channel breakdown and floodplain wetlands. *Geomorphology*, 118, 48–64.

Rayment, G.E., and Higginson, F.R., 1992. *Australian laboratory handbook of soil and water chemical methods*. Inkata Press, Sydney.

Formatted: Font: Italic

Revil, A., Karaoulis,M., Johnson, T., and Kemna, A., 2012. Review: some low-frequency electrical methods for subsurface characterization and monitoring in hydrogeology. *Hydrogeology Journal*, 20, 617–658.

Robertson, A., and Watts, R., 1999. Preserving Rural Australia. Csiro Publishing, 166p.

Saintilan, N., and Overton, I., 2010. *Ecosystem Response Modelling in the Murray-Darling Basin*. Csiro Publishing~~, 427p~~.

Formatted: Font: Italic

Sasaki, Y., 1992. Resolution of resistivity tomography inferred from numerical simulation. *Geophysical Prospecting*, 40, 453–46.

Schürch, M., and Buckley, D., 2002. Integrating geophysical and hydrochemical borehole-log measurements to characterize the Chalk aquifer, Berkshire, United Kingdom. *Hydrogeology Journal*, 10, 610–627.

Sharma, S.P., and Baranwal, V.C., 2005. Delineation of groundwater-bearing fracture zones in a hard rock area integrating very low frequency electromagnetic and resistivity data. *Journal of Applied Geophysics*, 57(2), 155–166.

Slater, L., 2007. Near surface electrical characterization of hydraulic conductivity: from petrophysical properties to aquifer geometries—a review. *Surveys in Geophysics*, 28, 169–197.

Sumanovac, F., and Dominkovic, S., 2007. Determination of resolution limits of electrical tomography on the block model in a homogenous environment by means of electrical modelling. *Rudarsko-Geolosko-Naftni Zbornik*, 19, 47–56.

Uhlemann, S.S., Sorensen, J.P.R., House, A.R., Wilkinson, P.B., Roberts, C., Goody, D.C., Binley, A.M., Chambers, J.E., 2016. Integrated time-lapse geoelectrical imaging of wetland hydrological processes. *Water Resources Research*, 52, 1607–1625.

Van Dijk, A.I.J.M., Beck, H.E., Crosbie, R.S., de Jeu, R.A.M., Liu, Y.Y., Podger, G.M., Timbal, B., and Viney, N.R., 2009. The Millennium Drought in southeast Australia (2001–2009): Natural and human causes and implications for water resources, ecosystems, economy, and society. *Water Resources Research*, 49, 1040–1057.

Viezzoli, A., Tosi, L., Teatini, P., and Silvestri, S., 2010. Surface water-groundwater exchange in transitional coastal environments by airborne electromagnetics: The Venice Lagoon example. *Geophysical Research Letters*, 37, L01402.

Wolfgang, C., 2000. *Hydrogeology of the Pilliga Sandstone, Coonamble Embayment and Water Resource Management*. PhD Thesis, Fenner School of Environment, The Australian National

Formatted: Font: Italic

737 University, Canberra.

738 TABLE 1

Depth	CGK	MQM54
0	silty loam	silty loam
0.5	medium clay	sandy clay
1	heavy clay	medium clay
1.5	heavy clay	medium clay
2	heavy clay	heavy clay
2.5	heavy clay	heavy clay
3	heavy clay	heavy clay
3.5	heavy clay	heavy clay
4	heavy clay	heavy clay
4.5	heavy clay	heavy clay
5	sandy clay	sandy clay
5.5	sandy clay	sandy clay
6	sandy clay	medium clay
6.5	sandy clay	medium clay
7	medium clay	sandy clay
7.5	heavy clay (saturated)	sandy clay
8	sandy clay (saturated)	sandy clay
8.5	sandy clay (saturated)	sandy clay (saturated)
9	Sand (saturated)	sandy clay (saturated)

739

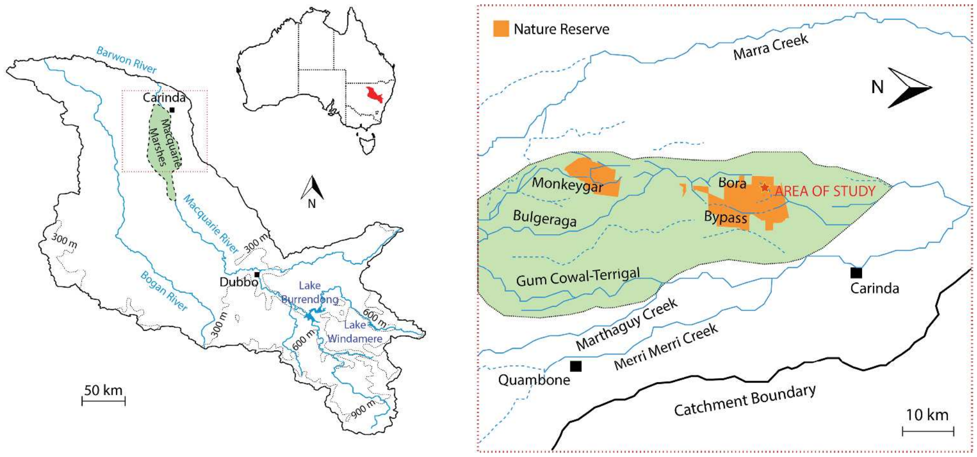

370x170mm (300 x 300 DPI)

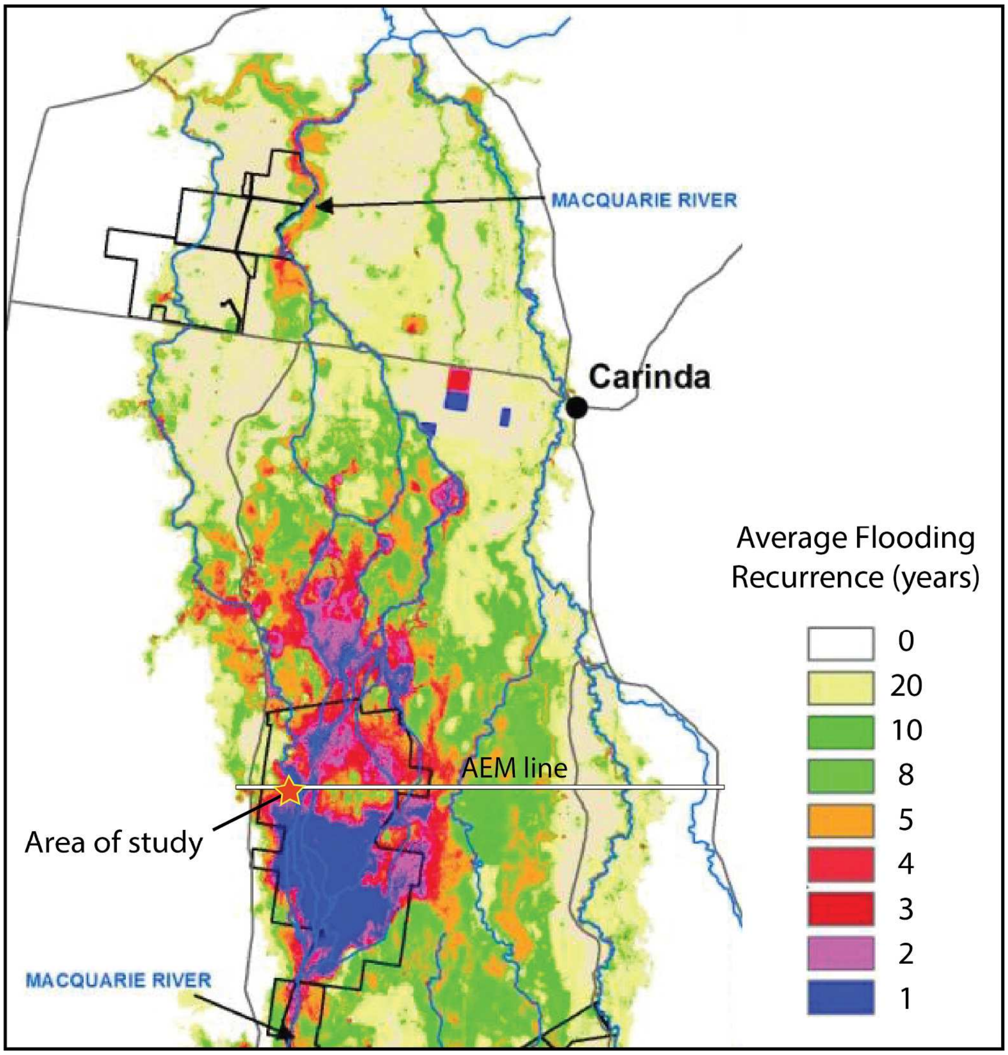

215x225mm (300 x 300 DPI)

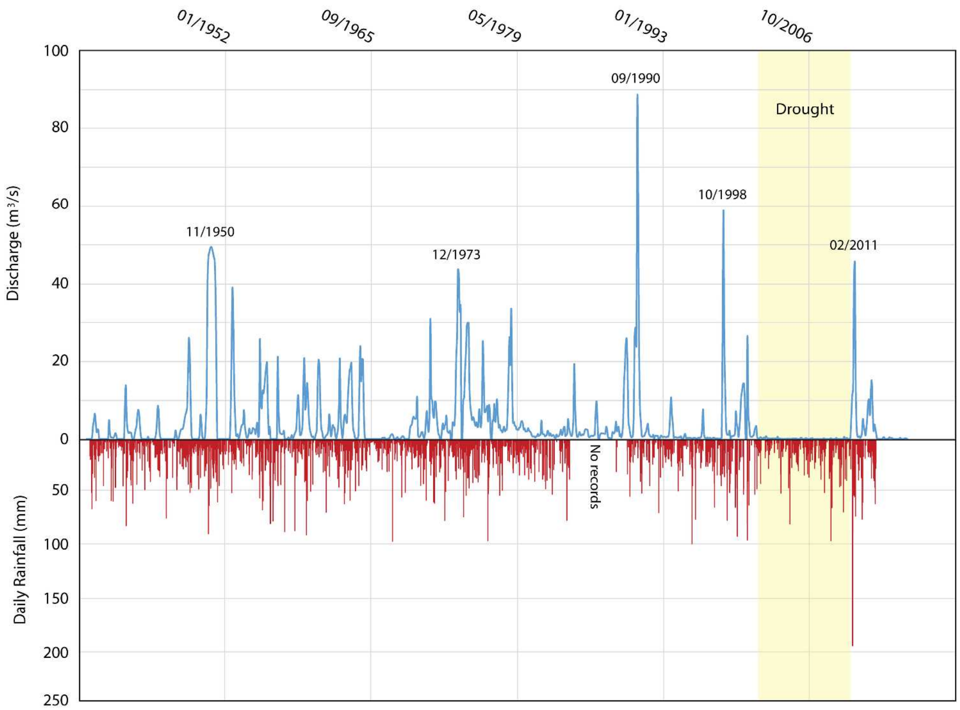

296x208mm (300 x 300 DPI)

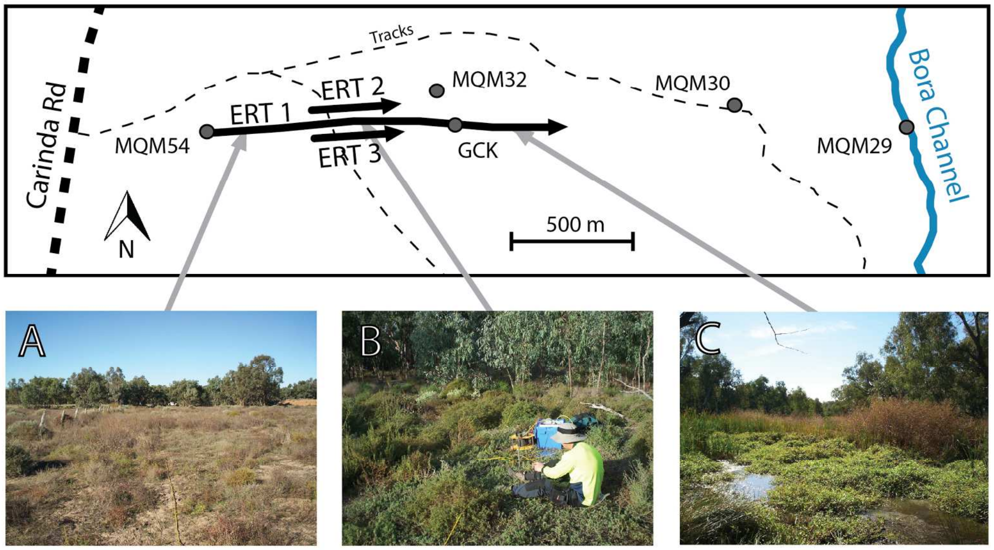

185x103mm (300 x 300 DPI)

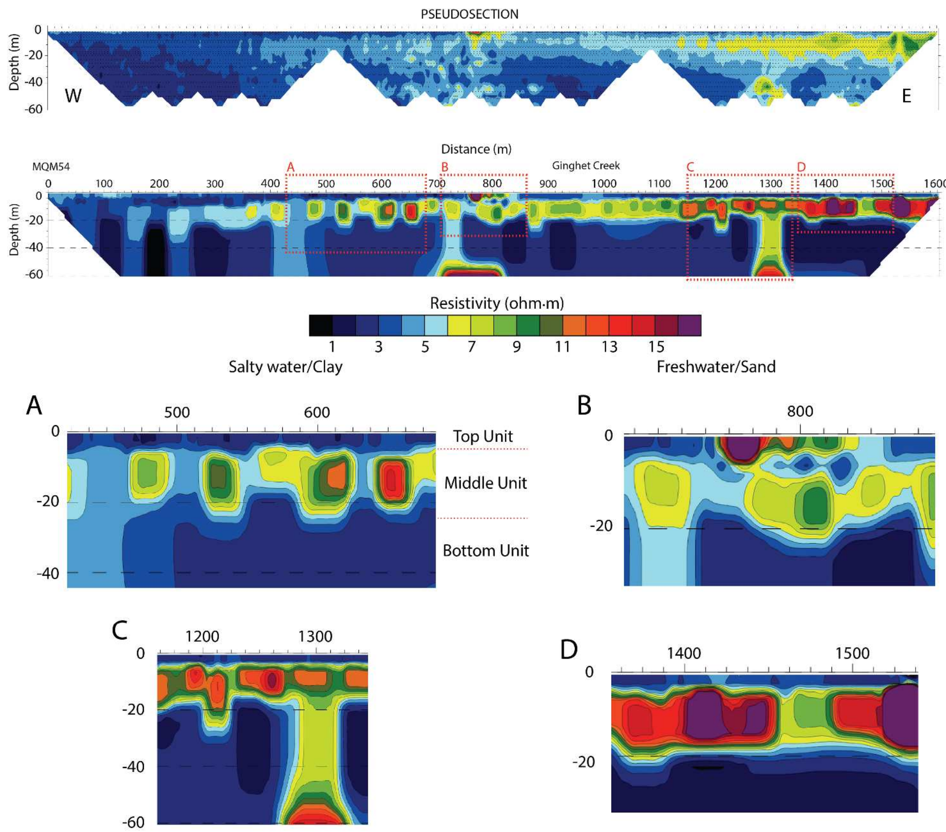

311x259mm (300 x 300 DPI)

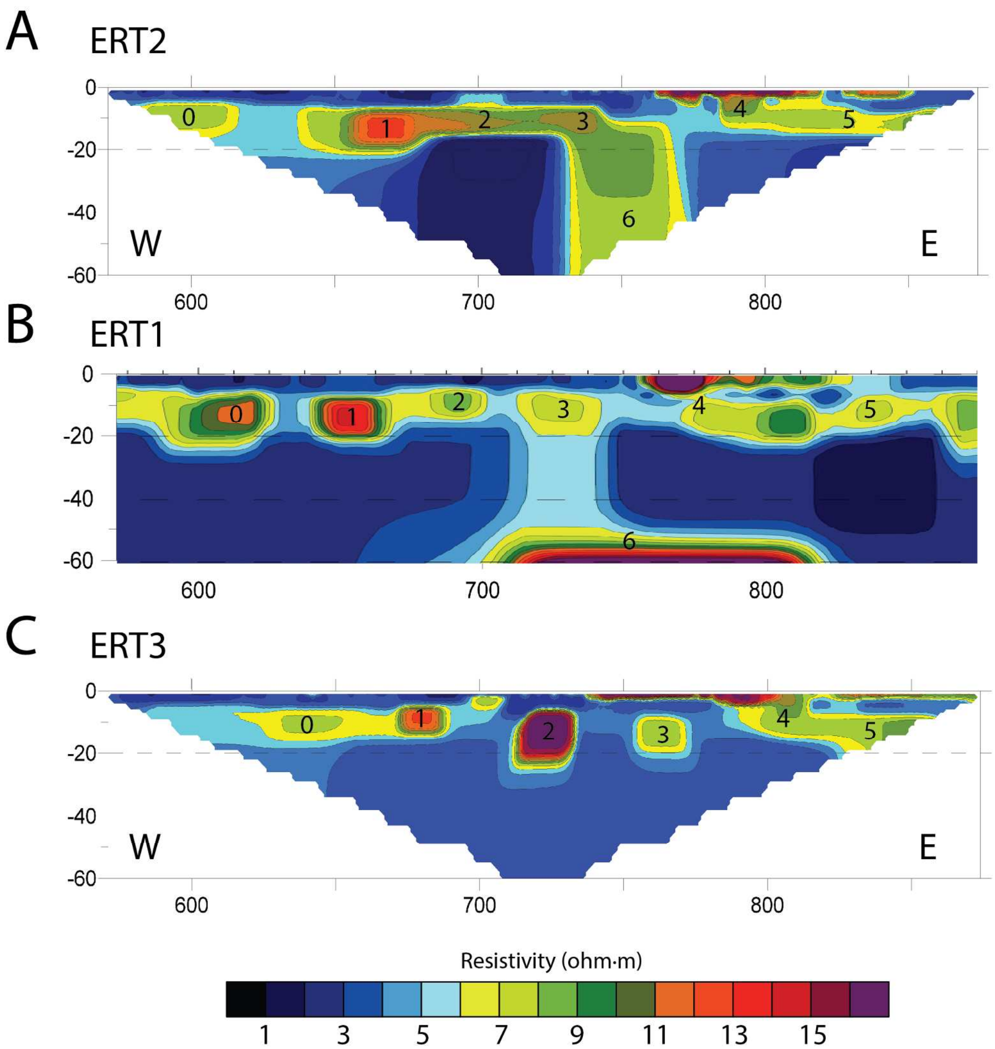

184x193mm (300 x 300 DPI)

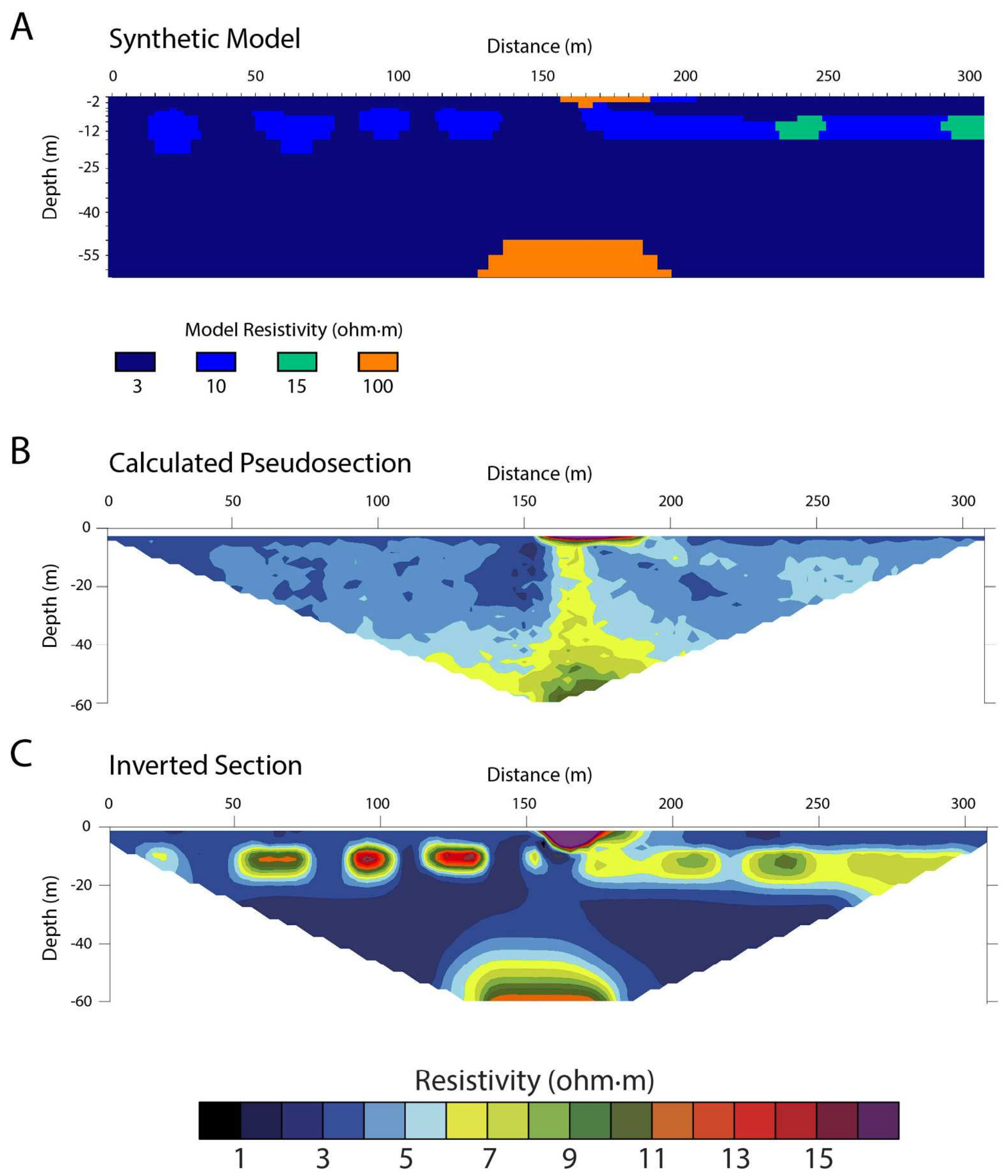

174x204mm (300 x 300 DPI)

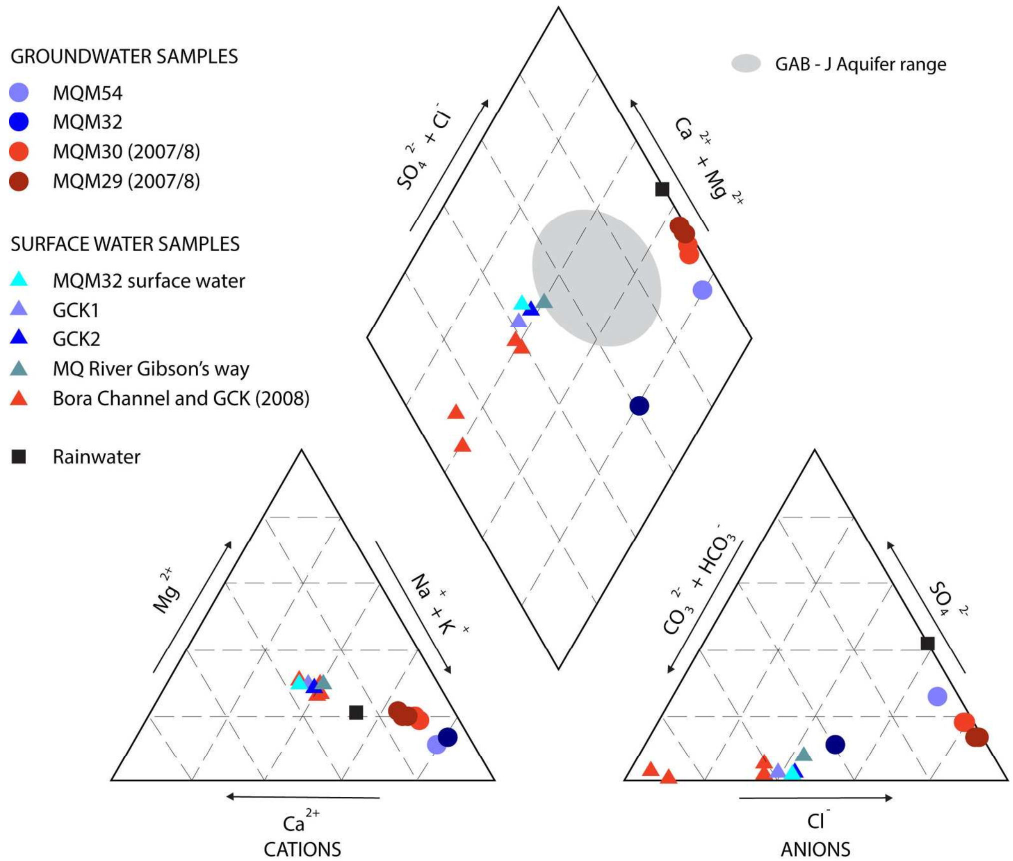

217x186mm (300 x 300 DPI)

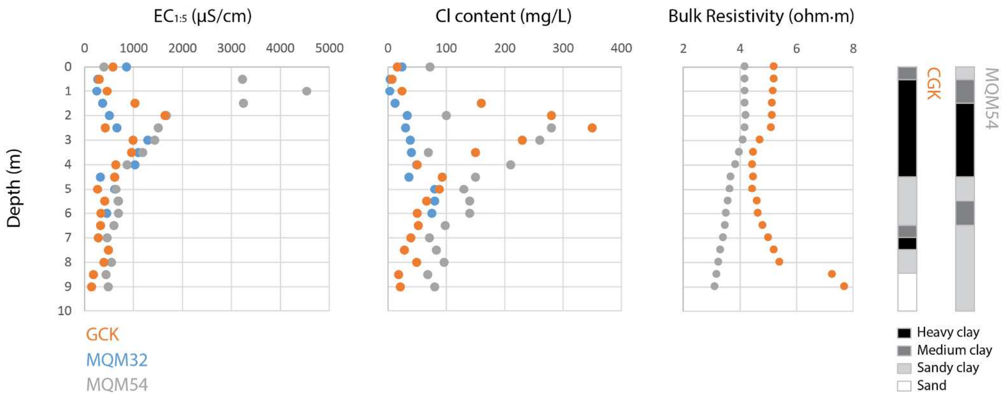

224x91mm (300 x 300 DPI)

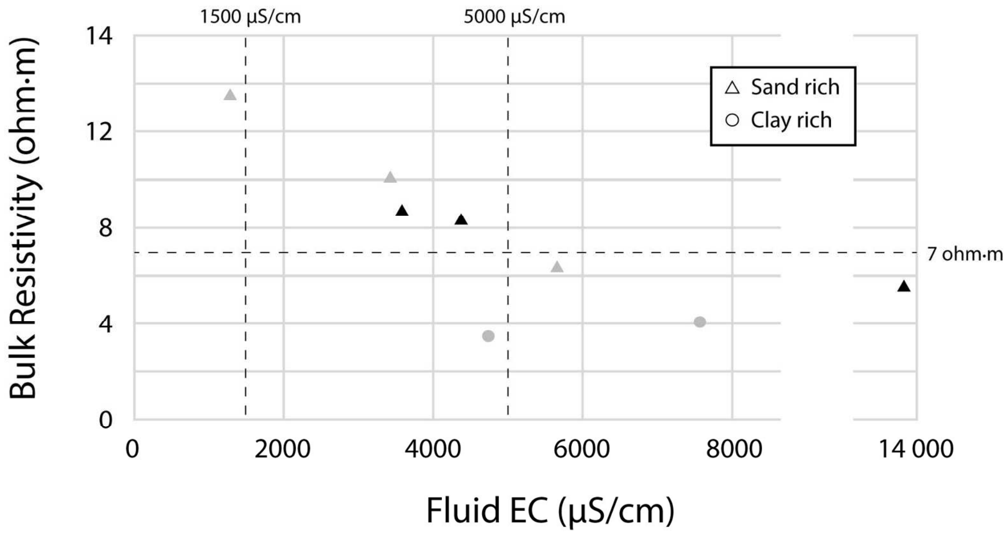

153x80mm (300 x 300 DPI)

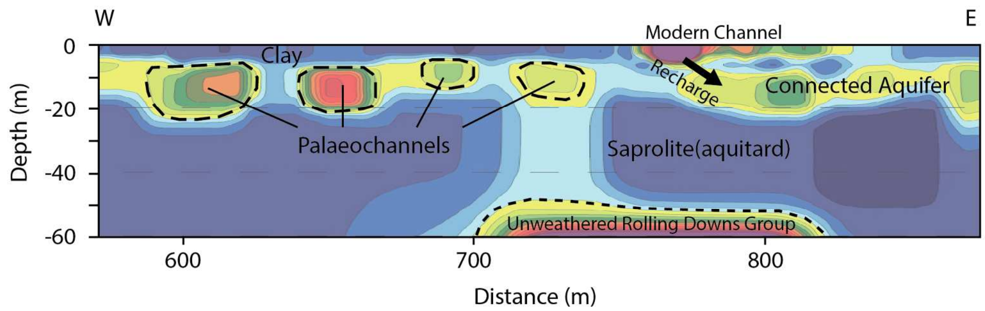

179x54mm (300 x 300 DPI)

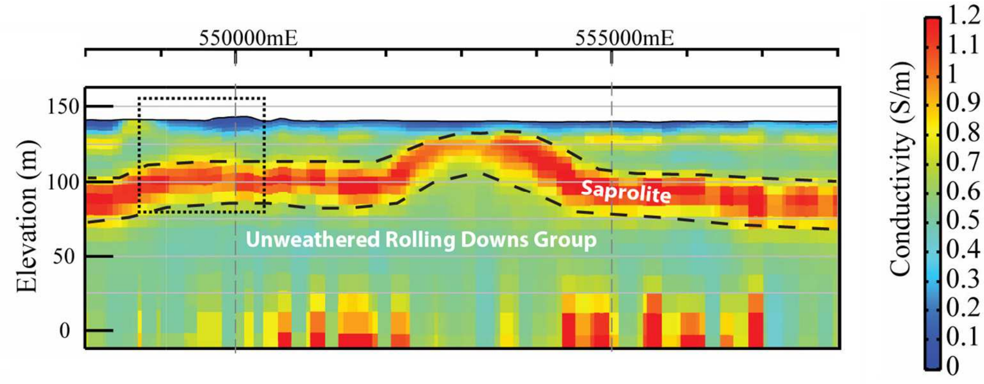

125x50mm (300 x 300 DPI)